Monovalent *Strep*-Tactin for strong and site-specific tethering in nanospectroscopy

Fabian Baumann[1], Magnus S. Bauer[1], Lukas F. Milles[1], Alexander Alexandrovich[2], Hermann E. Gaub[1] and Diana A. Pippig[1,3]*

Strep-Tactin, an engineered form of streptavidin, binds avidly to the genetically encoded peptide *Strep*-tag II in a manner comparable to streptavidin binding to biotin. These interactions have been used in protein purification and detection applications. However, in single-molecule studies, for example using atomic force microscopy-based single-molecule force spectroscopy (AFM-SMFS), the tetravalency of these systems impedes the measurement of monodispersed data. Here, we introduce a monovalent form of *Strep*-Tactin that harbours a unique binding site for *Strep*-tag II and a single cysteine that allows *Strep*-Tactin to specifically attach to the atomic force microscope cantilever and form a consistent pulling geometry to obtain homogeneous rupture data. Using AFM-SMFS, the mechanical properties of the interaction between *Strep*-tag II and monovalent *Strep*-Tactin were characterized. Rupture forces comparable to biotin:streptavidin unbinding were observed. Using titin kinase and green fluorescent protein, we show that monovalent *Strep*-Tactin is generally applicable to protein unfolding experiments. We expect monovalent *Strep*-Tactin to be a reliable anchoring tool for a range of single-molecule studies.

Specificity and exact control over the alignment and geometry of molecular constituents are prerequisites to successful nanospectroscopy experiments. For example, in single-molecule force spectroscopy (SMFS), the way in which the probed molecules (for example, proteins) are tethered largely influences the experimental performance as well as the reliability and interpretation of the data obtained. We aimed to adapt molecular interactions based on or related to avidin-like proteins to tackle this challenge and establish a versatile anchoring tool to study any protein of interest at the single-molecule level. After the discovery of avidin (A)[1,2] in 1940 and streptavidin (SA)[3] in 1964 as biotin sequestering proteins, their impact in biotechnology was quickly exploited[4,5]. With their outstanding femtomolar-range affinity towards biotin, the proteins found versatile application and rapidly became a molecular link between nano- and biotechnology, especially when the biotinylation of samples became accessible[6–8]. The biotin:SA/A interaction was the first molecular complex studied by atomic force microscopy (AFM)-based SMFS[9,10]. *Strep*-Tactin (ST) is an engineered SA[11] that specifically binds to the genetically encodable peptide *Strep*-tag II (amino acid sequence SII: WSHPQFEK). SII occupies the same binding site in SA and ST as biotin would[11,12]. The SII:ST system is predominantly used in protein purification[13], but also in affinity imaging and various *in vivo* applications[14–16].

The tetravalency in avidin-like proteins accounts for their striking avidity. Nevertheless, it can be disadvantageous to certain applications that rely on 1:1 stoichiometries. Stable, high-affinity monomeric forms of avidin-like proteins are challenging to obtain due to the interplay of the neighbouring subunits. Substantial protein engineering has given rise to monomeric SA variants with compromised binding properties[17]. Howarth and colleagues introduced a tetrameric, but monovalent SA (monoSA) with unimpaired biotin affinity. Key to this is the creation of a point-mutated SA construct that is incapable of binding biotin[18]. MonoSA is used in

structural biology[19,20], nanobiotechnology[21,22] and *in vivo* detection[23,24]. Similarly, applications for monovalent ST (monoST) arise, for example, *in vivo*, where biotin labelling is not always an option and working with genetically encoded SII is convenient. We introduce monoST with a single SII binding site and a unique cysteine (Cys) that confers either specific immobilization or fluorescence labelling. Monovalency is achieved by reassembling a heterotetrameric ST, analogous to monoSA[18]. Remarkably, we found the biotin-binding-deficient SA mutant equally unable to bind SII. MonoST thus consists of one functional ST subunit with a unique Cys residue, as well as three mutant SA subunits. Various applications of the construct, for example, as a fluorescence probe in the detection of SII-tagged targets in cells, can be envisioned. Here, we focus on the force-spectroscopic characterization of the SII:monoST interaction, thus establishing the pair as a reliable anchoring tool for various implementations of SMFS.

Other than bulk affinities, unbinding forces provide insight into the mechanical character of an interaction. Application-dependent, the tolerance of a complex to, for example, shear stress can be advantageous. Here, we present dynamic SMFS data of the SII:ST interaction obtained with an AFM, using a site-specifically immobilized monoST. SII-fused green fluorescent protein (GFP) and titin kinase (TK) constructs were probed to demonstrate the general applicability of this system in protein unfolding experiments. This is the first SMFS study of an SA-like protein exploiting an unambiguous tethering geometry. We expect monoST to find broad application in nanobiotechnology. As a force-spectroscopy tool, monoST offers deeper insight into, for example, the mechanism of the force-activation of mechano-sensitive enzymes.

Both biotin:SA/A as well as SII:ST have been investigated by force spectroscopy[9,10,25–27], and very high unbinding forces between biotin and SA/A have been reported. Owing to the tetravalency in SA/A and the measurement geometry, pinpointing the exact rupture

[1]Center for Nanoscience and Department of Physics, Ludwig Maximilians University of Munich, Amalienstraße 54, Munich 80799, Germany. [2]Randall Division of Cell and Molecular Biophysics and Cardiovascular Division, New Hunt's House, King's College London, London SE1 1UL, UK. [3]Center for Integrated Protein Science Munich, Ludwig Maximilians University of Munich, Butenandtstraße 5–13, Munich 81377, Germany. *e-mail: diana.pippig@physik.lmu.de
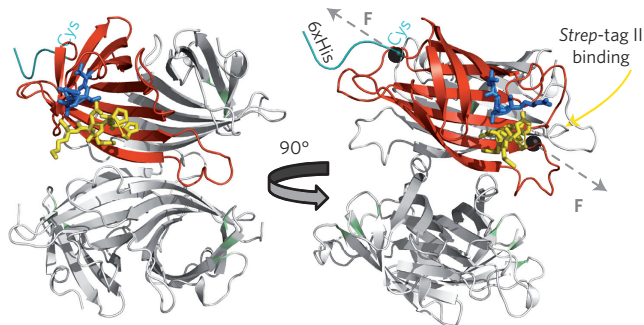
Figure 1 | Model of monoST based on the crystal structures of SA and ST. For SA, non-functional subunits adapted from protein data bank (PDB) entry 1RSU are depicted in grey, and residues N23A, S27D and S45A affecting biotin[18] as well as SII binding, when mutated, are highlighted in green. For ST, the functional subunit adapted from PDB entry 1KL3 is depicted in red, SII peptide is shown in yellow, the loop altered for ST compared to SA (residues 44–47: ESAV → VTAR) is highlighted in blue, with residues in a stick representation. The model is depicted from the top and rotated by 90° in side view. The hexa-His-tag and Cys residue opposite the SII binding site in the functional subunit are highlighted in cyan. Black spheres schematically represent anchor points, with corresponding directions of applied force in the AFM experiments. In the experiments, the probed proteins are fused to SII either with their N- or C-terminus.

forces of the interaction between biotin and a distinct subunit of the SA/A tetramer is challenging. In the case of ST, data from studies using ambiguous tethering geometries suggest that the force required to unbind SII from monoST is low compared to that in the biotin:SA/A interaction (37 pN, ref. 28; 20–115 pN, ref. 26). In AFM-SMFS, well-defined coupling strategies are desirable. Ideally, the interaction between a tethering molecule attached to the cantilever and a handhold-tag on the sample is strong to permit applicability to the various proteins to be probed[29–31]. A small handhold is less likely to interfere with the native protein fold of the sample. The SII:ST pair generally meets these requirements.

A unique Cys residue in monoST enables selective coupling

ST harbours four functional SII-binding subunits that are indistinguishable in their binding capacity. Selective coupling to the AFM

cantilever is not possible with this construct, and the tetravalency impedes the measurement of monodispersed force-spectroscopy data. We therefore engineered a monovalent ST heterotetramer with a single Cys that can be reacted to maleimido-polyethyleneglycol (PEG) functionalized surfaces, such as AFM cantilevers. To obtain uniform rupture force distributions, the monoST variant accommodates only one functional subunit. The remaining three subunits were adapted from monoSA, as established previously[18]. The structural model in Fig. 1 illustrates the composition of monoST. The functional subunit contains the Cys modification for selective immobilization, guaranteeing a consistent pulling geometry and thus homogeneous rupture data. As the Cys is located opposite the SII binding pocket of the β-barrel in the ST monomer, the force propagates through a single subunit (Fig. 1). If the other subunits were also functional, more complex pulling geometries and force-propagation scenarios would arise.

The structural integrity and stoichiometry of reconstituted monoST were verified by denaturing gel electrophoresis (Supplementary Fig. 1) and a GFP pull-down assay (Supplementary Fig. 2). The 1:3 ratio of functional-to-mutated subunits and accessibility of Cys were confirmed (Supplementary Fig. 1). For the SII binding test, ST constructs (tetra-, monovalent and fully mutated) were attached to a PEGylated glass surface via their Cys residue. GFP was pulled down in areas with functional ST. Increased fluorescence intensity coincided with immobilized tetraST compared to the monoST spot. This correlates with the anticipated SII binding capacities. No fluorescence signal, and thus GFP-SII interaction, was observed for the completely mutated construct. Aside from the capability of monoST to indeed bind a single SII-tagged GFP, this also confirms ST construct immobilization via Cys.

To determine the affinity of monoST to a SII-peptide and compare it to commercially available tetraST (IBA), isothermal titration calorimetry (ITC) measurements were conducted (Fig. 2). For both monoST and tetraST, the measured K_d for SII binding was ~2.3 μM. This compares well to published values (0.2/1.4 μM)[11,32]. The respective binding stoichiometry of four and one binding sites was confirmed in the experiment. Slight deviations from theoretical stoichiometries can be attributed to errors in determining the protein concentrations. Because the binding constants are deduced from the slope of the sigmoidal fit, a discrepancy in functional protein concentration should primarily affect the
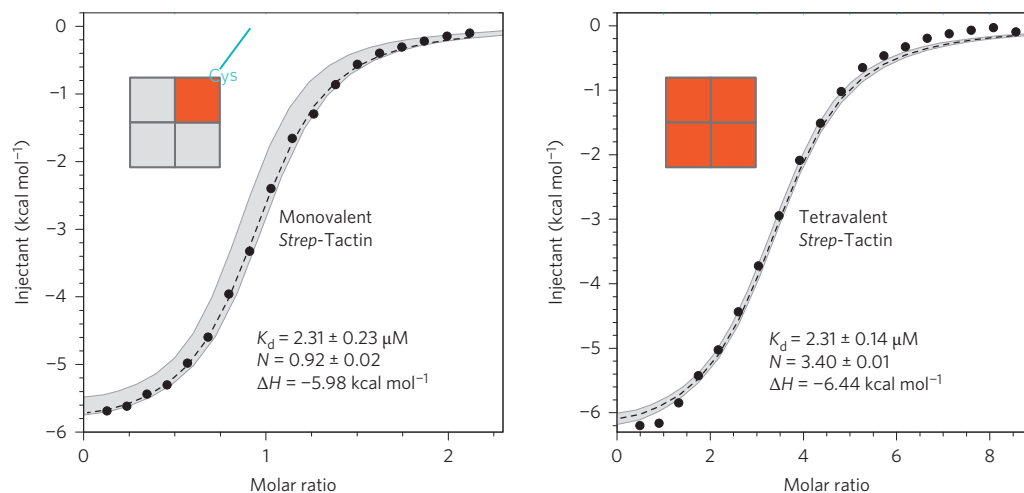

Figure 2 | ITC measurements of ST constructs and SII peptide. Data obtained for monoST (scheme with active, Cys-modified subunit in red and mutated subunits in grey) and tetraST (IBA, four functional subunits, red) were analysed by fitting a one-site binding model to obtain K_d, N (binding stoichiometry) and ΔH (enthalpy). The corresponding confidence interval of fits for three (monovalent) and five (tetravalent) data sets is depicted in grey. Errors were obtained from global fits of all data points of all respective data sets.
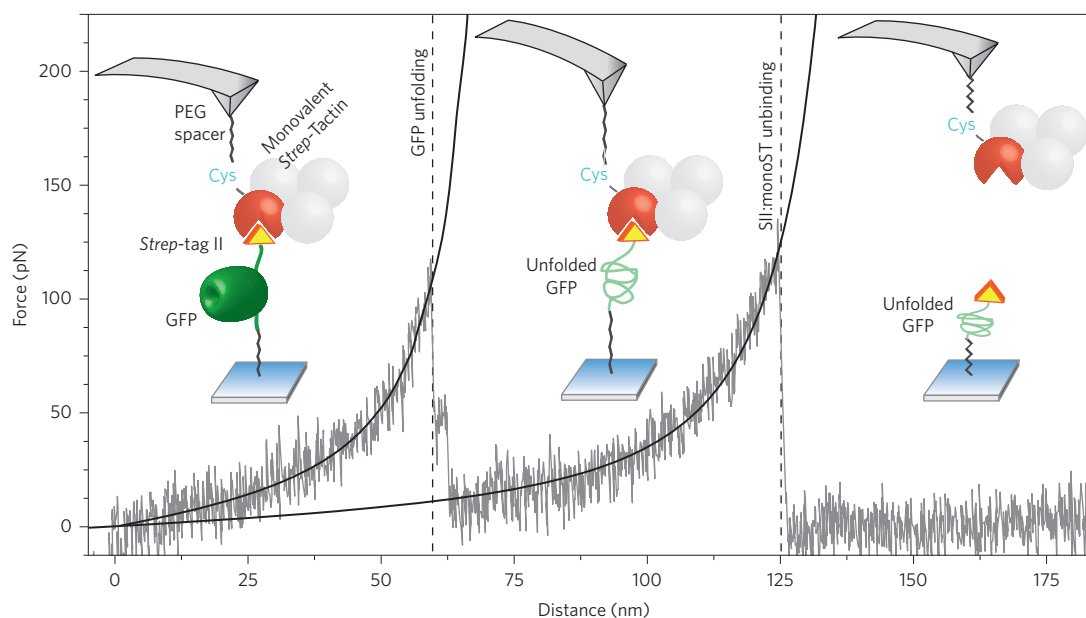
Figure 3 | Characterization of SII:monoST as a general handhold system in AFM-based SMFS. The scheme illustrates the measurement set-up with immobilized GFP harbouring a C-terminal SII and acting as a fingerprint domain. MonoST is represented by four spheres, three mutated, non-functional subunits are depicted in grey, the functional one in red. Each unfolding and rupture process is illustrated according to the observed, exemplary force–distance curve. Unfolding and rupture events are fitted according to the worm-like chain (WLC) model.

stoichiometry, not the K_d. The K_d for monoST binding to GFP with either an N- or C-terminal SII-tag, determined by ITC, is in the range of 1 μM. The fully mutated construct did not exhibit any measurable interaction.

Dynamic SMFS of the SII:monoST interaction

The SII:ST interaction was previously investigated in other contexts using SMFS. Moayed and colleagues[33] used a tandem repeat SII in an optical tweezer set-up that stretched DNA to compare different tethering methods. Tang and co-workers[28] used tetraST in AFM recognition imaging, giving an estimate of the unbinding force between SII and ST (37 pN at 337 pN s^{-1} loading rate). Kim et al.[26] probed the dynamic range of the interaction, providing SII-tagged protein fingerprint constructs (immunoglobulin-like domain I27 and SNase) at both the surface and the cantilever. Tethering was only achieved if an ST tetramer in solution connected two SII samples. In this way, two differentiated rupture force distributions were obtained for SII:ST unbinding. This can be attributed to the multiple binding site occupation scenarios in the asymmetric, dimeric substructure of the ST tetramer (four binding sites, two SII). Similarly, immobilized tetraST offers four different interaction sites and hence pulling geometries for SII.

Figure 3 presents the general arrangement of the present AFM experiment as well as an exemplary force versus distance curve displaying GFP unfolding and the final SII:monoST rupture. MonoST is specifically attached to the cantilever via the unique Cys of the functional subunit. The mutated subunits have no active means of interaction with the sample and are bypassed from the obvious path of force propagation. AFM-SMFS data analysis was intended to be semi-automated for minimal bias in the analysis. Specific SII:monoST binding and rupture events are clearly observed if GFP is unfolded. For the evaluation of the SII:monoST interaction, we therefore only considered curves with a single GFP unfolding event, fully exploiting the advantage of the GFP fingerprint in the experimental set-up and thus improving data reliability. Because the force drops back to almost zero as soon as the GFP is unfolded, it can be presumed that SII:monoST is not under load at that point. Accordingly, the observed rupture force distribution for SII:monoST

unbinding at a given loading rate after initial GFP unfolding is considered representative (Supplementary Fig. 3). Including single rupture events where the GFP was not unfolded did not significantly alter the measurement-derived data, but the statistics could be biased by taking non-specific events into account.

Unbinding forces vary for N- and C-terminal SII placement

GFP constructs were probed either with N- or C-terminally fused SII and it was found that only GFP with C-terminal SII is frequently unfolded (Supplementary Fig. 4). The strength of the SII:monoST interaction is thus dependent on tag placement and the pulling geometry arising from it (Fig. 4a). To verify this finding we also probed a low force fingerprint TK construct with an N-terminal SII-tag. We observed frequent TK kinase domain unfolding, with data yields comparable to the GFP experiment (Supplementary Fig. 5).

To evaluate the interaction and dynamic rupture force range between SII and monoST for GFP-SII and SII-TK constructs, we analysed representative data sets containing 8,774 and 4,933 retraction curves, respectively, for each of five distinct retraction velocities (200, 800, 2,000, 5,000 and 10,000 nm s^{-1}; Fig. 4). Figure 4b presents the most probable forces and respective loading rates for the final SII:monoST rupture and GFP unfolding in the case of construct GFP-SII for each retraction velocity set. From a fit according to the Bell–Evans model[34,35], the width of the binding potential Δx could be determined, yielding 0.50 nm for GFP unfolding and 0.23 nm for SII:monoST unbinding for the GFP-SII construct. The respective k_{off} values are 2.9×10^{-4} s^{-1} and 0.34 s^{-1}. For the SII-TK construct, Δx was determined to be twice as high (0.45 nm) as that for the C-terminally SII-tagged sample, which correlates well with the rupture forces dropping by a factor of two. The value of k_{off} is in a comparable range (0.60 s^{-1}). The force-spectroscopy-derived off rates for SII:monoST unbinding are comparable to surface plasmon resonance data (0.03–0.26 s^{-1})[32]. For the GFP-SII sample, the loading rate dependence fits for GFP unfolding and final rupture intersect one another; in other words, at low loading rates, the force required for GFP unfolding is more likely to exceed the SII:monoST rupture force. With increasing loading rates this behaviour is inverted. GFP unfolding at low
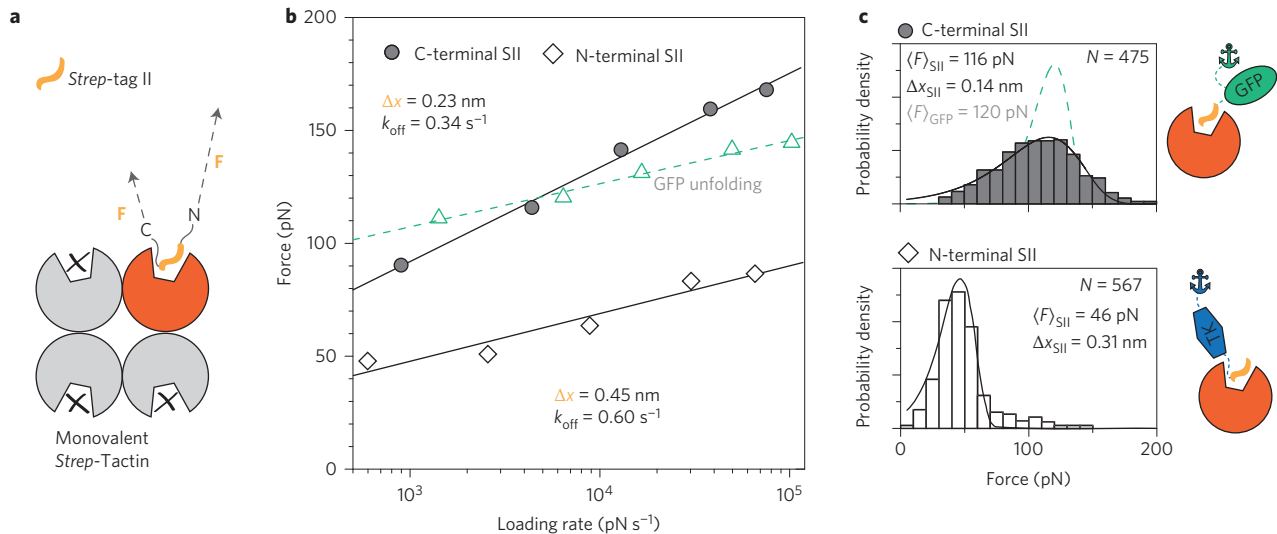
Figure 4 | Comparison of SII:monoST unbinding forces depending on the placement of SII on the termini of the probed protein. a, Schematic of monoST with SII occupying the functional binding site (based on PDB: 1KL3). The C-terminal part of SII is buried more deeply in the binding site than the N-terminal part. Generally, the two different attachments and thus pulling geometry scenarios can be expected to vary the SII:monoST unbinding forces. **b,** Dynamic force spectrum of the SII:monoST interaction for measurements with either N- or C-terminally fused SII. The force versus loading rate dependences of the SII:monoST rupture for a GFP construct with C-terminal SII (filled circles) in comparison to GFP unfolding (open green triangles), as well as for the SII:monoST rupture for a TK construct with N-terminal SII (open diamonds) are shown. Most probable rupture forces were obtained by fitting the rupture force histograms of each retraction velocity set with the Bell–Evans model. Loading rates were obtained by Gaussian fitting of values derived from the slope of individual extension traces. Only force–distance curves with a single GFP unfolding event or TK unfolding fingerprint were considered and evaluated. Δx and k_{off} were obtained by fitting data points according to the Bell–Evans model. The SII:monoST interaction is about half as strong at comparable loading rates when SII is N-terminally fused to the probed protein (here TK) compared with the C-terminal tag (here GFP). Accordingly, Δx is doubled for the weaker bond. **c,** Exemplary rupture force histograms for SII:monoST rupture at 800 nm s^{-1} retraction velocity in the AFM experiment. Top: data for the final rupture of C-terminally SII-tagged GFP (grey bars, solid line) and GFP unfolding (dashed green line). Bottom: data for the SII:monoST rupture of the N-terminally tagged TK construct (open bars, solid line). The presence of a few high force rupture events in the case of SII-TK may be attributed to a negligible number of unspecific attachment events via the Ig-like domains in the construct. Most probable rupture forces and Δx were derived from fitting data according to the Bell–Evans model.

loading rates is observed, owing to the inherently broader distribution of the SII:monoST rupture force (Fig. 4c and Supplementary Fig. 3). In the experimentally covered loading rate range, the rupture force distribution for the final SII:monoST rupture always coincides with the much narrower distribution for GFP unfolding. The most probable forces for SII:monoST rupture for the N-terminal SII construct are significantly lower than for GFP unfolding, which is in line with the observation that GFP is not suited to being a fingerprint when using N-terminal SII.

It is evident that the force distribution of the GFP unfolding is much narrower than that of SII:monoST unbinding. This is to be expected, as the potential width of the unfolding is much higher than that of the SII:monoST rupture (Fig. 4b,c). A fit of the histograms in Fig. 4c based on the standard Bell–Evans model results in Δx of ~0.29 and ~0.14 nm for unfolding and unbinding, respectively. For N-terminal SII, Δx is 0.31 nm. These values are slightly lower than those determined from the force loading rate dependence (Fig. 4b), for which only the peak positions of the force distributions are analysed. The narrow distribution of GFP unfolding forces suggests that instrument drift and cantilever aging are negligible (also compare Supplementary Fig. 7). The width of the SII:monoST rupture force histograms is thus inherent to the narrow binding potential and, as such, is a genuine property of this molecular pair in the given pulling geometry (C-terminal SII). Notably, this differs for an N-terminal SII, where lower unbinding forces and increased potential widths correlate with the broadened binding potential.

To verify the selectivity and reliability of the tethering established here, several control experiments were performed. SII-tagged GFP was compared to GFP fused with a GCN4-tag in AFM-SMFS. Significant sample interaction was only observed in probed areas

where GFP-SII was immobilized (Supplementary Fig. 6). When implementing an ST with four non-functional subunits, no significant interactions could be observed. The tethering specificity was also confirmed by competition, by adding 1 mM desthiobiotin during data collection. After adding the competitor, SII:monoST interactions became less abundant by far (Supplementary Fig. 6). This possibility of competing with the interaction is key to the system's use in affinity purification. The effect could also be relevant to other applications with monoST, for example, in the targeted release of SII-tagged ligands, as previously demonstrated with a cell-membrane-penetrating ST variant[36].

Previously, a rupture force distribution exhibiting two distinct maxima had been postulated for the SII:ST interaction (C-terminal SII constructs) by Kim and co-authors[26]. We did not observe two force regimes for the bond rupture between monoST and either SII-tagged GFP or TK. Using a selectively anchored monoST to bind a single SII exposed by the GFP or TK molecules on the surface eliminates the issue of inhomogeneous rupture force distributions. By offering only one binding site for the SII in an entirely unambiguous attachment geometry, monodisperse unbinding force distributions are to be expected.

We compared AFM-based force spectroscopy measurements using either specifically immobilized tetra- or monoST. A clear increase in single GFP-unfolding events as well as overall data yield was observed when using monoST (Supplementary Fig. 7 and Supplementary Table 1). TetraST measurements yielded about 2% single GFP-unfolding events, but about 8% were obtained for monoST. Using monoST proved much more reliable. With tetraST, periods of sparse interaction during the typically ~14 h measurements were observed, and cantilever wear was more

drastic (Supplementary Fig. 7). We attribute this effect to tearing of the tetrameric ST structure. This is in agreement with former SMFS studies on the disruption of the SA dimer interface, which was found to occur at ~100 pN (ref. 37). If high forces need to be probed, as in our exemplary GFP-unfolding experiment, monoST is a superior choice to conventional tetraST. Notably, because the mean rupture force for the (C-terminal)SII:monoST bond, even at low loading rates, still exceeds 50 pN, it can be assumed that the handhold pair is applicable to a broad range of mechanically stressed coupling reactions, such as in protein force spectroscopy studies.

Comparing the SII:monoST interaction strength with that of biotin:SA/A, we find that in a certain loading rate regime, the forces are in the same range[25]. The nonlinearity that is observed for the biotin:SA/A rupture, which is representative of the presence of more than one energy barrier along the unbinding coordinate, was not found for the SII:monoST interaction. This may be due to the limited loading rate range covered in the present experiments. Considering the altered conformation in the loop proximal to the ligand binding pocket in ST compared with SA, differences in the unbinding energy landscape would also not be unexpected[38]. The discrepancy in equilibrium stability versus rupture force between the two complexes biotin:SA and SII:monoST probably originates from the minor change in the loop region on top of the binding pocket. For SA, this loop undergoes substantial conformational changes upon biotin binding to close up the binding site like a lid. This movement is not observed in ST upon SII-binding. Furthermore, this loop closure has been concluded to be partially responsible for the outstanding off rates, and thus for the K_d value found for biotin:SA[39]. Additionally, SA variants such as the so-called 'traptavidin' exist, in which the introduction of slight alterations in this loop region lead to a stabilized closed form and thus even lower dissociation rate constants[40]. As the unbinding force is dominated by the primary interactions between ligand and binding pocket, the 'lid closure effect' may have little influence. Thus, the mode of forced ligand unbinding would be comparable in biotin:SA and SII:ST, despite their vastly differing equilibrium stabilities. In addition, biotin or SII affinity may be influenced by the properties of the molecule to which they are attached[41]. It is worthwhile noting that none of the hitherto published biotin:SA/A force spectroscopy studies used a completely specific attachment strategy for either binding partner (for example, biotinylated bovine serum albumin or microspheres, as well as non-specifically attached SA). While not exhibiting any obvious disadvantages over biotin, SII represents an attractive alternative to probe proteins in a comparable force range. In many instances, the genetically encoded peptide tag is preferable to a biotin modification, which requires additional coupling and purification steps after protein expression. Another advantage of using SII as a handhold rather than a biotin modification lies in their respective affinities to ST and SA. Their K_d values differ tremendously (micromolar for SII:ST versus femtomolar for biotin:SA)[11,18,41]. Thus, when probing SII-tagged protein the cantilever is less prone to get clogged than when using biotinylated protein, as even trace amounts of free biotin or non-covalently coupled biotinylated protein can block the cantilever, nearly irreversibly.

Conclusions

We have established a robust tethering strategy applicable to and adaptable by a broad range of nanotechnology applications. Such stable biomolecular complexes are needed in AFM-based or other force spectroscopy techniques. The use of genetically encoded SII as a handhold is superior to those that require post-translational modification (for example, biotin or digoxigenin). The strength of its interaction with monoST renders the pair an excellent choice for such applications. Remarkably, the difference in binding strength when using SII on either the N- or C-terminus could only be identified as a consequence of the high specificity of our tethering system and the superb understanding and control its pulling geometry provides. As this renders the SII:monoST interaction a tunable rupture force system, other implementations may arise, for example, in 'single-molecule cut & paste'[42]. Finally, the modification of ST to hold a unique immobilization and single functional SII binding site boosts the robustness and applicability of the system. Fluorescently labelled monoST may be used, for example, for super-resolution microscopy, exploiting the advantage of the 1:1 stoichiometry. Other applications, such as in structural biology and more general fluorescence imaging and tracking, should also be feasible, as the extremely high affinity found for biotin:SA is not a general necessity for such implementations. MonoST builds on the prevalence and popularity of SA and ST and therefore enables the probing of readily available protein constructs with improved specificity and stability.

Methods

Methods and any associated references are available in the online version of the paper.

References

1. Eakin, R. E., McKinley, W. A. & Williams, R. J. Egg-white injury in chicks and its relationship to a deficiency of vitamin H (biotin). *Science* **92,** 224–225 (1940).
2. Gyorgy, P. & Rose, C. S. Cure of egg-white injury in rats by the 'toxic' fraction (avidin) of egg white given parenterally. *Science* **94,** 261–262 (1941).
3. Tausig, F. & Wolf, F. J. Streptavidin—a substance with avidin-like properties produced by microorganisms. *Biochem. Biophys. Res. Commun.* **14,** 205–209 (1964).
4. Bayer, E. A., Skutelsky, E., Wynne, D. & Wilchek, M. Preparation of ferritin–avidin conjugates by reductive alkylation for use in electron microscopic cytochemistry. *J. Histochem. Cytochem.* **24,** 933–939 (1976).
5. Heggeness, M. H. & Ash, J. F. Use of the avidin–biotin complex for the localization of actin and myosin with fluorescence microscopy. *J. Cell Biol.* **73,** 783–788 (1977).
6. Bayer, E. A., Zalis, M. G. & Wilchek, M. 3-(*N*-maleimido-propionyl)biocytin: a versatile thiol-specific biotinylating reagent. *Anal. Biochem.* **149,** 529–536 (1985).
7. Schatz, P. J. Use of peptide libraries to map the substrate specificity of a peptide-modifying enzyme: a 13 residue consensus peptide specifies biotinylation in *Escherichia coli. Nature Biotechnol.* **11,** 1138–1143 (1993).
8. Beckett, D., Kovaleva, E. & Schatz, P. J. A minimal peptide substrate in biotin holoenzyme synthetase-catalyzed biotinylation. *Protein Sci.* **8,** 921–929 (1999).
9. Moy, V. T., Florin, E. L. & Gaub, H. E. Intermolecular forces and energies between ligands and receptors. *Science* **266,** 257–259 (1994).
10. Florin, E. L., Moy, V. T. & Gaub, H. E. Adhesion forces between individual ligand–receptor pairs. *Science* **264,** 415–417 (1994).
11. Voss, S. & Skerra, A. Mutagenesis of a flexible loop in streptavidin leads to higher affinity for the *Strep*-tag II peptide and improved performance in recombinant protein purification. *Protein Eng.* **10,** 975–982 (1997).
12. Schmidt, T. G., Koepke, J., Frank, R. & Skerra, A. Molecular interaction between the *Strep*-tag affinity peptide and its cognate target, streptavidin. *J. Mol. Biol.* **255,** 753–766 (1996).
13. Schmidt, T. G. & Skerra, A. The *Strep*-tag system for one-step purification and high-affinity detection or capturing of proteins. *Nature Protoc.* **2,** 1528–1535 (2007).
14. Nampally, M., Moerschbacher, B. M. & Kolkenbrock, S. Fusion of a novel genetically engineered chitosan affinity protein and green fluorescent protein for specific detection of chitosan *in vitro* and *in situ. Appl. Environ. Microbiol.* **78,** 3114–3119 (2012).
15. Knabel, M. *et al.* Reversible MHC multimer staining for functional isolation of T-cell populations and effective adoptive transfer. *Nature Med.* **8,** 631–637 (2002).
16. Moosmeier, M. A. *et al.* Transactin: a universal transmembrane delivery system for *Strep*-tag II-fused cargos. *J. Cell. Mol. Med.* **14,** 1935–1945 (2010).
17. Lim, K. H., Huang, H., Pralle, A. & Park, S. Stable, high-affinity streptavidin monomer for protein labeling and monovalent biotin detection. *Biotechnol. Bioeng.* **110,** 57–67 (2013).
18. Howarth, M. *et al.* A monovalent streptavidin with a single femtomolar biotin binding site. *Nature Methods* **3,** 267–273 (2006).

19. Lau, P. W. *et al*. The molecular architecture of human Dicer. *Nature Struct. Mol. Biol.* **19,** 436–440 (2012).
20. Sauerwald, A. *et al*. Structure of active dimeric human telomerase. *Nature Struct. Mol. Biol.* **20,** 454–460 (2013).
21. Howarth, M. *et al*. Monovalent, reduced-size quantum dots for imaging receptors on living cells. *Nature Methods* **5,** 397–399 (2008).
22. Carlsen, A. T., Zahid, O. K., Ruzicka, J. A., Taylor, E. W. & Hall, A. R. Selective detection and quantification of modified DNA with solid-state nanopores. *Nano Lett.* **14,** 5488–5492 (2014).
23. Sonntag, M. H., Ibach, J., Nieto, L., Verveer, P. J. & Brunsveld, L. Site-specific protection and dual labeling of human epidermal growth factor (hEGF) for targeting, imaging, and cargo delivery. *Chemistry* **20,** 6019–6026 (2014).
24. Xie, J. *et al*. Photocrosslinkable pMHC monomers stain T cells specifically and cause ligand-bound TCRs to be 'preferentially' transported to the cSMAC. *Nature Immunol.* **13,** 674–680 (2012).
25. Merkel, R., Nassoy, P., Leung, A., Ritchie, K. & Evans, E. Energy landscapes of receptor–ligand bonds explored with dynamic force spectroscopy. *Nature* **397,** 50–53 (1999).
26. Kim, M., Wang, C. C., Benedetti, F. & Marszalek, P. E. A nanoscale force probe for gauging intermolecular interactions. *Angew. Chem. Int. Ed.* **51,** 1903–1906 (2012).
27. Chilkoti, A., Boland, T., Ratner, B. D. & Stayton, P. S. The relationship between ligand-binding thermodynamics and protein–ligand interaction forces measured by atomic force microscopy. *Biophys. J.* **69,** 2125–2130 (1995).
28. Tang, J. *et al*. Recognition imaging and highly ordered molecular templating of bacterial S-layer nanoarrays containing affinity-tags. *Nano Lett.* **8,** 4312–4319 (2008).
29. Puchner, E. M. *et al*. Mechanoenzymatics of titin kinase. *Proc. Natl Acad. Sci. USA* **105,** 13385–13390 (2008).
30. Li, Y. D., Lamour, G., Gsponer, J., Zheng, P. & Li, H. The molecular mechanism underlying mechanical anisotropy of the protein GB1. *Biophys. J.* **103,** 2361–2368 (2012).
31. Zocher, M. *et al*. Single-molecule force spectroscopy from nanodiscs: an assay to quantify folding, stability, and interactions of native membrane proteins. *ACS Nano* **6,** 961–971 (2012).
32. Schmidt, T. G. *et al*. Development of the twin-*Strep*-tag(R) and its application for purification of recombinant proteins from cell culture supernatants. *Prot. Expr. Purif.* **92,** 54–61 (2013).
33. Moayed, F., Mashaghi, A. & Tans, S. J. A polypeptide–DNA hybrid with selective linking capability applied to single molecule nano-mechanical measurements using optical tweezers. *PLoS ONE* **8,** e54440 (2013).
34. Evans, E. & Ritchie, K. Dynamic strength of molecular adhesion bonds. *Biophys. J.* **72,** 1541–1555 (1997).
35. Bell, G. I. Models for the specific adhesion of cells to cells. *Science* **200,** 618–627 (1978).
36. Moosmeier, M. A., Bulkescher, J., Hoppe-Seyler, K. & Hoppe-Seyler, F. Binding proteins internalized by PTD-fused ligands allow the intracellular sequestration of selected targets by ligand exchange. *Int. J. Mol. Med.* **25,** 557–564 (2010).
37. Kim, M. *et al*. Nanomechanics of streptavidin hubs for molecular materials. *Adv. Mater.* **23,** 5684–5688 (2011).
38. Korndorfer, I. P. & Skerra, A. Improved affinity of engineered streptavidin for the *Strep*-tag II peptide is due to a fixed open conformation of the lid-like loop at the binding site. *Protein Sci.* **11,** 883–893 (2002).
39. Weber, P. C., Ohlendorf, D. H., Wendoloski, J. J. & Salemme, F. R. Structural origins of high-affinity biotin binding to streptavidin. *Science* **243,** 85–88 (1989).
40. Chivers, C. E. *et al*. A streptavidin variant with slower biotin dissociation and increased mechanostability. *Nature Methods* **7,** 391–U376 (2010).
41. Malmstadt, N., Hyre, D. E., Ding, Z., Hoffman, A. S. & Stayton, P. S. Affinity thermoprecipitation and recovery of biotinylated biomolecules via a mutant streptavidin-smart polymer conjugate. *Bioconjug. Chem.* **14,** 575–580 (2003).
42. Pippig, D. A., Baumann, F., Strackharn, M., Aschenbrenner, D. & Gaub, H. E. Protein–DNA chimeras for nano assembly. *ACS Nano* **8,** 6551–6555 (2014).

Author contributions

H.E.G. and D.A.P. conceived the idea and designed the experiments. Experiments were carried out and evaluated by F.B., M.S.B. and D.A.P. L.F.M. provided force spectroscopy evaluation software and advice. A.A. prepared TK. D.A.P. wrote the manuscript with input from all authors.

Additional information

Supplementary information is available in the online version of the paper. Reprints and permissions information is available online at www.nature.com/reprints. Correspondence and requests for materials should be addressed to D.A.P.

Competing financial interests

The authors declare no competing financial interests.

Methods

A full description of experimental details can be found in the Supplementary Information. In brief, ST and mutant SA (deficient in SII binding) constructs were cloned into pET vectors (Merck Millipore), if applicable with a hexa-His-tag and Cys or without for the non-functional subunits that were not meant to attach to the AFM-cantilever surface. ST and mutant SA with and without the extra Cys were expressed separately in *E. coli* BL21(DE3)-CodonPlus. The constructs formed inclusion bodies that were isolated as described previously[18,43].To reconstitute monoST and to provide a 1:3 ratio of functional ST to non-functional SA in the final tetramer, inclusion bodies were solubilized in 6 M guanidinium chloride and then mixed in a 1:10 ratio before refolding and purification, which was accomplished by means of the His-Tag on the Cys-modified subunit. Stoichiometry and the binding affinity between monoST and an SII-peptide were analysed by ITC. To characterize the SII:monoST interaction and as a proof of general applicability of the pair, we used it with GFP and TK in a dynamic AFM-SMFS experiment. Passivation of the sample surfaces, here the glass coverslip and the AFM cantilever, was ensured by heterobifunctional PEG spacers used for specific sample immobilization[44,45]. Covalent and site-selective attachment of the protein to be probed was achieved using the ybbR-tag/Sfp-synthase system, which has been successfully used in recent force spectroscopy measurements[46–48]. This reaction is highly efficient with N- or C-terminally ybbR-tagged proteins. Cys-modified monoST was immobilized on maleimido-PEG 5000 (M_w = 5,000 Da) functionalized BioLever Mini cantilevers (Olympus)[49]. One GFP construct harboured an N-terminal ybbR-tag for surface immobilization and a C-terminal SII for recognition by the monoST-decorated cantilever tip. For control measurements, a construct harbouring a GCN4-tag instead of SII was used. GFP was attached to a PEG5000-coenzymeA (CoA) modified glass surface via the ybbR-tag (Sfp catalysed)[47]. Protein coupling to the CoA/PEG-surface was achieved under saturating conditions, so the density of coupled GFP was adjusted by using a fraction of non-reactive CH$_3$-PEG5000.

The ratio of maleimido(CoA)-PEG5000 to CH$_3$-PEG5000 was chosen such that the surface density gave rise to a high yield of single-tethering event curves. A fraction of curves devoid of any interaction is acceptable for the sake of improved automated data sorting, evaluation and to obtain fewer multi-event curves. GFP constructs were cloned with their respective tags (ybbR and SII or GCN4-tag) into pGEX vectors (GE Healthcare) and expressed in *E. coli* BL21(DE3)-CodonPlus (Agilent Technologies). Purification was achieved by GST- and His-tag based affinity chromatography. The GST-tag was removed from the final construct. Constructs with an N-terminal SII-tag, SII-GFP-ybbR and a titin kinase construct (SII-TK-ybbR) were implemented accordingly in force spectroscopy experiments.

References

43. Schmidt, T. G. & Skerra, A. One-step affinity purification of bacterially produced proteins by means of the '*Strep* tag' and immobilized recombinant core streptavidin. *J. Chromatogr. A* **676,** 337–345 (1994).
44. Jain, A., Liu, R., Xiang, Y. K. & Ha, T. Single-molecule pull-down for studying protein interactions. *Nature Protoc.* **7,** 445–452 (2012).
45. Celik, E. & Moy, V. T. Nonspecific interactions in AFM force spectroscopy measurements. *J. Mol. Recogn.* **25,** 53–56 (2012).
46. Limmer, K., Pippig, D. A., Aschenbrenner, D. & Gaub, H. E. A force-based, parallel assay for the quantification of protein–DNA interactions. *PLoS ONE* **9,** e89626 (2014).
47. Otten, M. *et al.* From genes to protein mechanics on a chip. *Nature Methods* **11,** 1127–1130 (2014).
48. Beckmann, A. *et al.* A fast recoiling silk-like elastomer facilitates nanosecond nematocyst discharge. *BMC Biol.* **13,** 3 (2015).
49. Zimmermann, J. L., Nicolaus, T., Neuert, G. & Blank, K. Thiol-based, site-specific and covalent immobilization of biomolecules for single-molecule experiments. *Nature Protoc.* **5,** 975–985 (2010).

Monovalent *Strep*-Tactin for strong and site-specific tethering in nanospectroscopy

Fabian Baumann, Magnus S. Bauer, Lukas F. Milles, Alexander Alexandrovich, Hermann E. Gaub, Diana A. Pippig*

*diana.pippig@physik.lmu.de

The experiments described in the manuscript were performed on custom-built AFMs, the details of which may be found in Gumpp *et al.*[1] This supporting information specifies methods, materials and additional data that are relevant for the conduction of the measurements discussed in the main text.

Preparation of the Strep-tagII Fusion Constructs

A superfolder Green Fluorescent Protein (GFP)[2] construct was designed to harbour an N-terminal ybbR-tag (DSLEFIASKLA)[3, 4] and a C-terminal Strep-tagII (SAWSHPQFEK = SII). The GFP gene was PCR amplified from a synthetic template (Lifetechnologies, Paisley, UK) with primers containing the respective tag coding sequences. The construct was cloned into a modified pGEX6P2 vector (GE Healthcare, Little Chalfont, UK) that, in addition to the GST-tag, harbours a 6xHis-Tag and a TEV-Protease cleavage site, by means of NdeI and XhoI restriction sites. The resulting fusion protein (ybbR-GFP-SII) harboured a GST- as well as a 6xHis-tag and was expressed in *E.coli* BL21(DE3)-CodonPlus cells (Agilent Technologies, Inc., Santa Clara, CA, USA). For this, 1 l of SB medium was inoculated with 10 ml of an overnight culture and grown at 37 °C. When an OD_{600} of 0.7 had been reached, over night expression at 18 °C was induced by adding 0.25 mM IPTG. Cells were lysed in 50 mM Tris HCl pH 7.5, 150 mM NaCl, 2 mM DTT, 5% Glycerol, by sonication. The ybbR-GFP-SII construct was obtained in the soluble fraction and purified by Glutathione affinity chromatography on a GSTrap column (GE Healthcare, Little Chalfont, UK). During over night incubation with PreScission protease the GST-tag was removed and the protein further purified by Ni-IMAC over a HisTrap HP column (GE Healthcare, Little Chalfont, UK). The purified protein was dialyzed against 50 mM Tris HCl pH7.5, 150 mM NaCl, 2 mM DTT, 5% Glycerol and then stored at -80 °C at a final concentration of ~12 μM. The control construct ybbR-GFP-GCN4 was prepared accordingly[5]. Further, a SII-GFP-ybbR construct and a Titin Kinase construct with identical tag placement (SII-TK-ybbR) were prepared and purified by Ni-IMAC and in addition size exclusion chromatography for the TK construct. The TK construct was expressed in insect cells. All proteins were used at comparable concentrations for surface conjugation.


Preparation of Monovalent Strep-Tactin (monoST)

Two Strep-Tactin (ST) constructs were designed: one harbouring an intact SII binding site and an N-terminal 6xHis-tag as well as a unique Cysteine (Cys) residue. The other one resembled a Streptavidin variant that had formerly been shown to not bind biotin anymore and still assemble in the tetrameric structure[6]. Both ST variants were PCR amplified from synthetic templates (Centic, Heidelberg, Germany) and cloned into pET vectors. Expression was, similar to the GFP construct, achieved in 300 ml and 700 ml SB cultures of transformed *E. coli* BL21(DE3)-CodonPlus, respectively. The harvested cell pellets were treated separately in the beginning and dissolved in 4 ml per 1 g cell mass B-

S2

PER. After addition of Lysozyme and DNase cells were fully lyzed by sonification. Insoluble cell debris as well as inclusion bodies were sedimented by centrifugation at 20000 g for 30 min. After discarding the supernatant the inclusion body containing pellet was again resuspended in 4 ml / 1 g washing buffer (30 mM Tris HCl pH 7.5, 150 mM NaCl and 0.1% TritonX-100). Centrifugation and washing of the inclusion bodies were repeated four times, when the supernatant appeared fairly cleared. The inclusion bodies containing the Cys-modified functional ST were then dissolved in 6 ml solubilization buffer (20 mM Tris HCl pH 7.5, 6 M Guanidinium HCl), the ones containing the non-functional and untagged variant in 12 ml. After determining the protein concentration in the solubilized fractions by measuring the absorbance at 280 nm, the entire amount of non-functional ST was used and mixed with the volume equivalent of a tenth in mass of the latter with functional 6xHis-mono-Cys-ST. The mixed solubilized protein was again subjected to centrifugation for 30 min at 20000 g and the supernatant with the unfolded ST constructs collected. To accomplish refolding the mixture was slowly and drop-wise added to a stirred reservoir of 500 ml 1x PBS and 10 mM β-Mercaptoethanol (the use of DTT or the more expensive TCEP as reducing agents is also possible, if compatible with the Ni2+-column matrix used for the following His-Tag affinity purification step). The mixture was stirred over night at 4 °C to maximize refolding of the mixed ST. Next, the 500 ml protein sample was filtered through a cellulose filter to remove precipitate and then loaded onto a 5 ml HisTrap FF column (GE Healthcare) for Ni-IMAC purification. Elution of the reassembled monoST was achieved by a linear gradient from 10 to 300 mM Imidazole (in 1x PBS, 10 mM β-Mercaptoethanol). Elution fractions were analysed in gel electrophoresis. If the samples were not heated in gel loading dye prior to loading them onto the gel the protein remained a tetramer during gel electrophoresis. For samples that were incubated at 95 °C for 5 min in gel loading dye, the subunits were separated and subunits migrated separately as monomers (Supplementary Fig. S1). Thus, the stoichiometry of functional (slightly larger due to the 6xHis-tag and additional Cys) and non-functional (non-tagged) ST could be assessed. As intended by using a 10fold excess of non-functional, non-tagged construct, the ratio of functional to non-functional ST appears to be 1:3 (Supplementary Figure S1). Samples were pooled after elution from the affinity column and dialyzed against 1x PBS. As free reducing agent in the storage buffer would later on interfere with Mal-PEG immobilization of the monoST, bead-immobilized TCEP was added to the protein inside the dialysis tubing. ST was long-term stored at 4 °C in presence of TCEP beads. Generally, yields of 20 mg of purified protein per 1 l (300 ml for expression of His-tagged, functional protein, which is the yield affecting constituent) culture could be obtained.

For control experiments a tetramer harbouring a non-functional 6xHis-tagged and Cys-modified subunit in addition to the three unmodified non-functional ones was prepared accordingly (Supplementary Figure S1). Further, a variant containing four functional subunits with one harbouring a 6xHis-tag and a Cys was produced for comparison.

S3

Typically, final protein concentrations ranged around 14 µM. To verify Cys accessibility for cantilever immobilization, the ST constructs were reacted to Maleimido-ATTO647N and analysed by gel electrophoresis. As expected only the large 6xHis and Cys containing subunit is labelled (Supplementary Fig. S1) and reactivity towards surface coupled PEG-Maleimide should be comparably efficient.
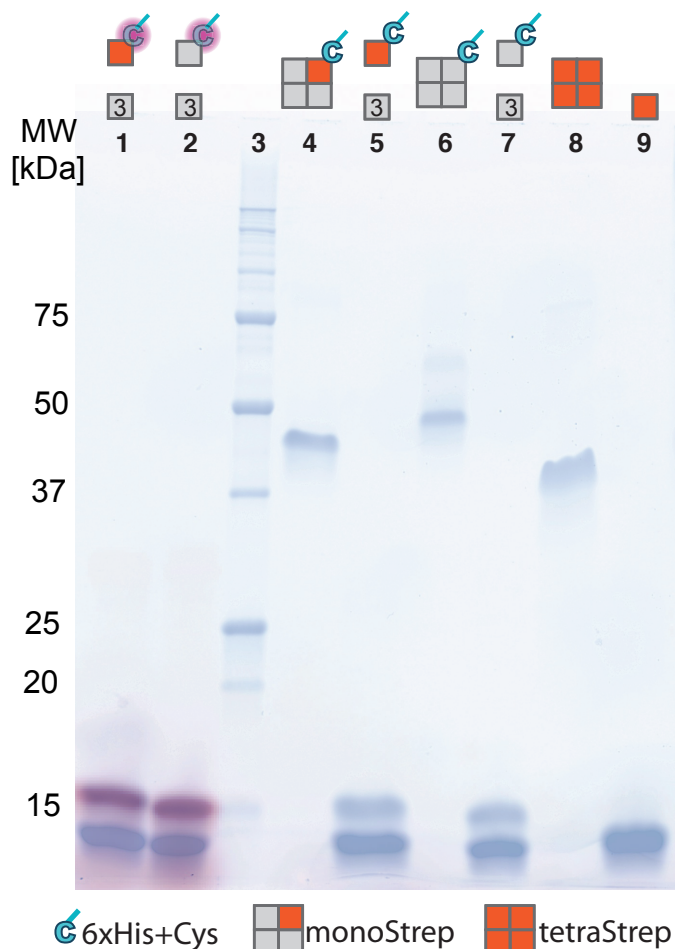
Supplementary Figure S1. SDS PAGE gel of refolded ST variants. MonoST and the non-functional variant were successfully refolded to form a heterotetramer (lanes 4/5 and 6/7, not heated and treated at 95 °C for 5 min in loading buffer, respectively) consisting of non-functional ST and functional 6xHis-Cys-ST or non-functional 6xHis-Cys-ST, respectively, in an estimated 3:1 ratio. For comparison, lanes 8 and 9 show the commercially available tetraST (IBA, Göttingen) homotetramer (not heated - 8; heat treated - 9). Cys-accessibility was tested by reacting Maleimide-ATTO647N to the refolded and purified hetero-tetramers (lane 1: monovalent, lane 2: non-functional mutant – consisting of four mutated subunits, one harbouring an extra Cys and 6xHis-Tag). Functional subunits are depicted in red, mutated ones in grey, the additional Cys residue as well as the 6xHis-Tag are highlighted in cyan.

S4

Strep-Tactin Immobilization and ybbR-GFP-SII Pull-down

As a control, modified ST constructs tetraST, monoST and the completely mutated variant that is supposedly not capable of binding the SII, were immobilized on the same PEG-Maleimide functionalized glass surface (same chemistry as used for the cantilever coupling). After washing off unreacted protein, SII-tagged GFP was incubated on the surface for 15 min. After rinsing off unbound GFP, the fluorescence on the surface was evaluated (Supplementary Fig. S4.). Whereas for the spot with the binding pocket mutant no signal was detected (max. signal: ~2000 counts, background range), the tetraST spot yielded a GFP signal (max. signal: 60000 counts) that was higher than at the spot were monoST (max. signal: ~15000 counts) was immobilized that also showed GFP binding (Supplementary Fig. S2).
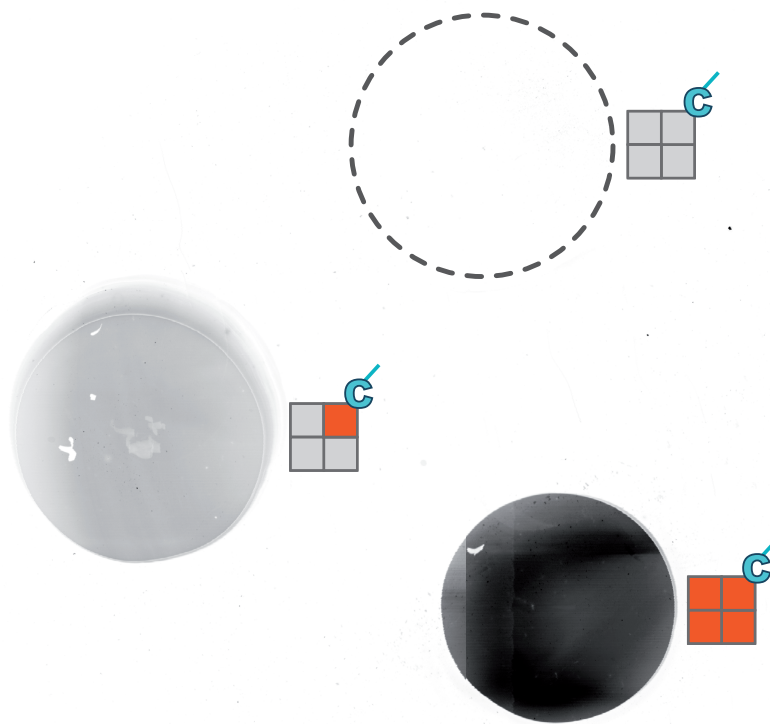
Supplementary Figure S2. Cys-modified ST variants were coupled to the same glass surface via PEG-Maleimide and incubated with ybbR-GFP-SII. The fully non-functional ST is not capable of binding SII-tagged GFP, whereas the monovalent construct appears to bind less GFP molecules than the tetravalent construct. Functional subunits are depicted in red, mutated ones in grey, the additional Cys residue as well as the 6xHis-Tag are highlighted in cyan.

Affinity Measurements

To avoid background effects from varying protein storage buffers, all protein samples were desalted and the buffer exchanged to the respective measurement buffer in MicroSpin columns (Thermo Scientific). The peptides were dissolved in 1x PBS. Affinities were determined by Isothermal Titration Calorimetry on a MicroCal iTC$_{200}$ instrument (Malvern, Worcestershire, UK). ST constructs were provided in a volume of 250 µl in the measurement cell (IBA ST at 12 µM and monoST at 56 µM). SII peptide (IBA, Göttingen) was titrated in from a stock concentration of 440 µM and 630 µM respectively, to account for the difference in binding stoichiometry between the ST variants (4 vs. 1 binding site). Data were fit with a one-site binding model in OriginPro (OriginLab, Northampton, UK) to obtain K_d values as well as the binding stoichiometry. We further tried to measure affinities in more sensitive fluorescence polarization assays. However since the fluorophore on the SII peptide seems to increase the affinity to ST and due to observed unspecific interactions of ST with glass and plastic ware those measurements were not considered reliable enough. One conclusion could still be drawn from these experiments: While we observed binding for the functional ST variants the fully mutated construct did not seem to significantly interact with the labelled peptide even at high concentrations (much higher than for the functional constructs). Thus, proper determination of the K_d with ITC was not considered feasible.

Preparation of Cantilevers

Cantilevers (BioLever Mini obtained from Olympus, Japan) were oxidized in a UV-ozone cleaner (UVOH 150 LAB, FHR Anlagenbau GmbH, Ottendorf-Okrilla, Germany) and silanized by soaking for 2 min in (3-Aminopropyl)dimethylethoxysilane (ABCR, Karlsruhe, Germany; 50% v/v in Ethanol). Subsequently, they were washed in toluene, 2-propanol and ddH$_2$O and dried at 80 °C for 30 min. After incubating the cantilevers in sodium borate buffer (pH 8.5), a heterobifunctional PEG crosslinker[7, 8] with N-hydroxy succinimide and maleimide groups (MW 5000, Rapp Polymere, Tübingen, Germany) was applied for 30 – 60 min at 25 mM in sodium borate buffer. Afterwards, monoST was bound to the cantilevers at room temperature for 1 h. Finally the cantilevers were washed and stored in 1x PBS.

Preparation of Glass Surfaces

S6

Glass cover slips were sonicated in 50% (v/v) 2-propanol in ddH$_2$0 for 15 min and oxidized in a solution of 50% (v/v) hydrogen peroxide (30%) and sulfuric acid for 30 min. They were then washed in ddH$_2$O, dried in a nitrogen stream and then silanized by soaking for 1 h in (3-Aminopropyl)dimethylethoxysilane (ABCR, Karlsruhe, Germany, 1.8% v/v in Ethanol). Subsequently, they were washed twice in 2-propanol and ddH$_2$O and dried at 80 °C for 40 min. After incubation in sodium borate buffer (pH 8.5), a heterobifunctional PEG crosslinker with N-hydroxy succinimide and maleimide groups (MW 5000, Rapp Polymere, Tübingen, Germany) mixed 2:1 with mono-functional NHS-PEG-CH3 (MW 5000, Rapp Polymere, Tübingen) was applied for 1 h at 25 mM in sodium borate buffer. After rinsing the surfaces, 20 mM Coenzyme A (Calbiochem) in coupling buffer (sodium phosphate, pH 7.2) was added on top of the surfaces to react with the maleimide groups. Protein was coupled to the surface after removal of residual CoA by adding a mix of e.g. 8 µl 11 µM ybbR-GFP-SII, 1 µl Sfp-Synthase (133 µM)[5, 9] and 1 µl of 10x reaction buffer (100 mM Tris pH 7.5, 100 mM MgCl2) and incubation for 2 h at room temperature. Surfaces were rinsed in 1x PBS prior to the measurement to prevent unbound protein to block the cantilever.

It should be noted, that it is also possible to couple protein from cruder samples or cell lysates directly to the surface, as the ybbR/CoA/Sfp chemistry is highly selective and reactive[9]. Purification of protein samples utilizing the anyway attached SII is also possible. Generally, residual biotin or desthiobiotin from expression media, cell extract or elution buffer should get disposed of by thoroughly rinsing the surface after protein immobilization. Trace amounts of these competitors can be further scavenged by addition of Neutravidin to the measurement buffer, that sequesters biotin but does not interact with Strep-Tactin[10].

AFM Measurements

A custom built AFM head and an Asylum Research MFP3D controller (Asylum Research, Santa Barbara, USA), which provides ACD and DAC channels as well as a DSP board for setting up feedback loops, were used. Software for the automated control of the AFM head and xy-piezos during the force spectroscopy measurements was programmed in Igor Pro (Wave Metrics, Lake Oswego, USA). BioLever Mini (BL-AC40TS) cantilevers (Olympus, Japan; 10 nm nominal tip radius, sharpened probe) were chemically modified (see Preparation of Cantilevers) and calibrated in solution using the equipartition theorem[11,12]. Dynamic force spectroscopy data was collected employing five different retraction velocities: 200, 800, 2000, 5000 and 10000 nm/s. To minimize unspecific interaction and since the on-rate of SII:monoST is in the time-scale of contact between probe and sample surface, no dwell times were employed. The contact time between functionalized AFM probe and the protein surface (ranging between ~5 and 70

ms) is therefore only determined by the retraction velocity, approach velocity (3000 nm/s), the indentation force (180 pN) and the substrate stiffness. The surface is sampled in steps of 100 nm distance.

Typically datasets containing between 5000 and 9000 force vs. distance curves per retraction velocity were collected. Curves were sorted by employing certain force and distance cut-offs, mainly restricting the low force regime to minimum 30 pN (for GFP-SII), as otherwise automated data evaluation was hampered by noise peaks. For SII-TK data was selected by correlating the recurring, characteristic TK kinase unfolding fingerprint. Rupture forces were evaluated from AFM force vs. distance curves utilizing a quantum mechanically corrected WLC model[13] (force spectroscopy data was evaluated in Python 2.7). Loading rates of individual unfolding/rupture events were determined by fitting the respective slope prior to the force peak (last 3 nm). For GFP constructs, in the final evaluation only curves with a single unfolded GFP, i.e. two peaks (1st: GFP-unfolding, 2nd: SII:monoST rupture) were considered. A distinction between specific and unspecific rupture events for single peak curves was not feasible. This is also not considered crucial, as the GFP fingerprint acts as an internal selection criterion and quality control. It can be assumed, that the force nearly drops back to zero when GFP is unfolded and that the SII:monoST interaction does not memorize the afore-sensed force. It also does not undergo irreversible or slowly reversing conformational changes under force load (otherwise repetitive probing of different molecules on the surface with the same monoST molecule on the cantilever would not be feasible). Generally, characteristic fingerprints should be obtained when using the SII:monoST pair to characterize arbitrary proteins concerning their unfolding behaviour.

Final rupture forces for each velocity set were binned to histograms that were fitted with the Bell-Evans model[14, 15] yielding the most probable rupture force (Supplementary Fig. S3). The average loading rate was determined by a Gaussian fit of the binned distribution for each retraction velocity. The most probable rupture force vs. loading rate dependency could be fitted according to the standard Bell-Evans model ($f(r)=(k_BT/\Delta x)\ln(\Delta x\, r/k_BTk_{off})$) to yield the width of the binding potential Δx and the dissociation rate k_{off} at zero force for the SII:monoST interaction.
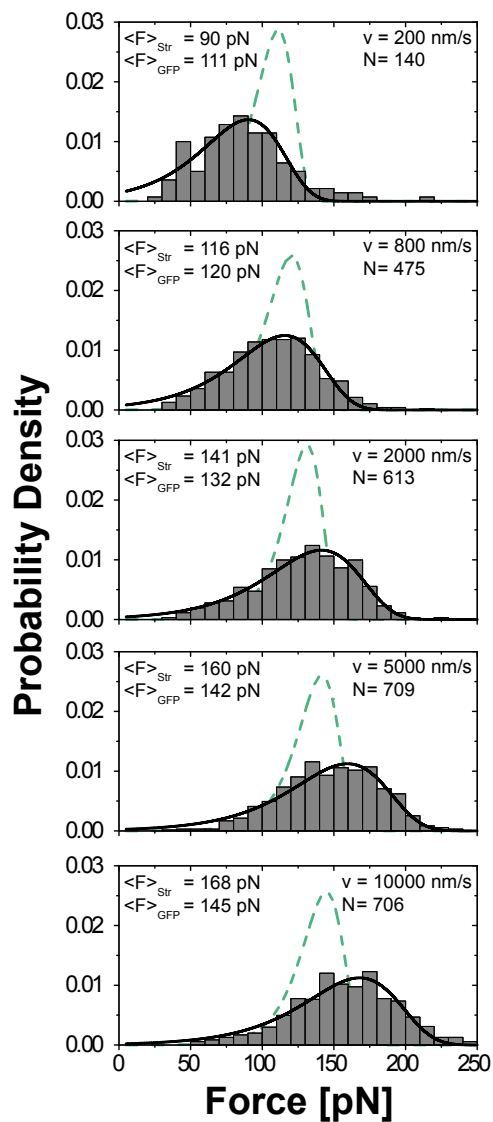
When using GFP as a fingerprint, due to the distribution of rupture force probabilities, we found a drop in the amount of observed GFP-unfolding events at low loading rates (Supplementary Fig. S3, compare N=140 at 200 nm/s and N=706 at 10000 nm/s), which should not affect the derived values for the most probable rupture force. In support of this, the rupture force histograms are clearly monodisperse and do not exhibit any sudden cut-off in the low force regime that would indicate loss of substantial data (Fig. 4C, Supplementary Fig. S3).

We further tested, whether placing SII on either terminus of the protein in question alters the SII:ST unbinding behavior. When comparing N- and C-terminally labeled GFP, we indeed observed significantly fewer GFP unfolding events when using an N-terminally

S8

SII-tagged construct (Supplementary Fig. S4). For comparison, only considering single GFP unfolding events, we found 8.3 % out of 3250 curves total for ybbR-GFP-SII and 0.4 % GFP unfolding events out of 3840 curves in total SII-GFP-ybbR. Analysis of the loading rate dependence of the final rupture force was not feasible for the SII-GFP-ybbR data due to the low number of events. With the reduced rupture force between N-terminally fused SII and monoST, GFP turned out to be too robust to act as a reliable fingerprint in aid of distinction of specific from unspecific interactions. *I.e.* the rupture force distributions inherent to GFP unfolding and to the SII:monoST interaction appear to not overlap sufficiently in this specific case of an N-terminal SII fusion.

As GFP unfolds at fairly high forces around 100 pN it can be considered a rather robust fingerprint. Thus, when studying other proteins of interest they might exhibit specific unfolding patterns at much lower forces.

As another example and to utilize a specific fingerprint in a lower force range, we studied a Titin Kinase (TK) construct. In this case SII was also placed N-terminally and the ybbR-tag fused to the C-terminus. We could show that the tethering strategy works equally well for this protein sample. Data yields compare to the GFP experiment and the specificity of SII:monoST as handhold pair is evident as we frequently see the low force kinase domain unfolding fingerprint (Supplementary Fig. S5). In addition, this experiment shows that SII can be utilized as either N- or C-terminal fusion, although rupture forces are decreased for N-terminal SII (Supplementary Fig. S4 and Fig. 4). Supplementary Figure S5 depicts a superposition of 1730 TK unfolding curves. While the Kinase domain is frequently fully unfolded, we rarely observe Immunoglobulin (Ig)-like domain unfolding. This is in agreement with the ~200 pN known to be required for Ig-domain unfolding, which exceeds the unbinding force distribution for SII:monoST rupture. Further, this emphasizes the capacity and specificity of the system, as frequent Ig-like domain unfolding should be only occurring when pulling non-specifically.

Plot annotations (top to bottom):

Panel 1: $\langle F \rangle_{Str}$ = 90 pN, $\langle F \rangle_{GFP}$ = 111 pN, v = 200 nm/s, N= 140

Panel 2: $\langle F \rangle_{Str}$ = 116 pN, $\langle F \rangle_{GFP}$ = 120 pN, v = 800 nm/s, N= 475

Panel 3: $\langle F \rangle_{Str}$ = 141 pN, $\langle F \rangle_{GFP}$ = 132 pN, v = 2000 nm/s, N= 613

Panel 4: $\langle F \rangle_{Str}$ = 160 pN, $\langle F \rangle_{GFP}$ = 142 pN, v = 5000 nm/s, N= 709

Panel 5: $\langle F \rangle_{Str}$ = 168 pN, $\langle F \rangle_{GFP}$ = 145 pN, v = 10000 nm/s, N= 706

Supplementary Figure S3. Evaluation of AFM SMFS data for the interaction between GFP-SII and monoST. Only force-distance curves with a single GFP unfolding event were considered and evaluated. Rupture force histograms for SII:monoST rupture (grey bars and solid line) and GFP unfolding (dashed green line) at different retraction velocities in the AFM experiment are depicted.

S10
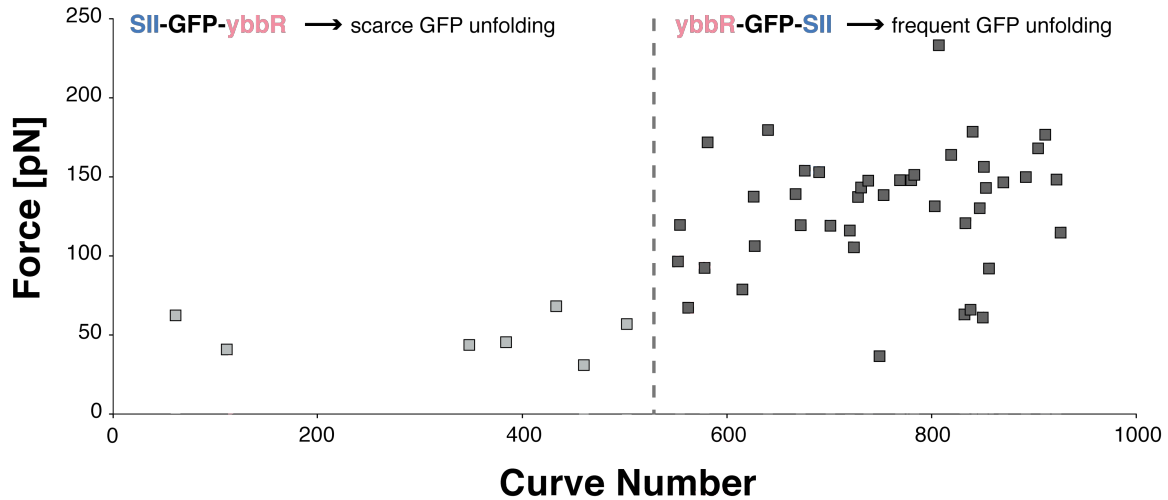
Supplementary Figure S4. Comparison of force spectroscopy data with respect to Strep-tag II attachment at either N- or C-terminus of GFP. Only with a C-terminal Strep-tag II high enough rupture forces between the tag and the monoST at the cantilever are achieved to frequently unfold GFP. Data was collected with the same cantilever. Events obtained at a retraction velocity of 5000 nm/s are shown. Evaluating data from five different retraction velocities yields: 8.3 % GFP unfolding events out of 3250 curves total for ybbR-GFP-SII and 0.4 % GFP unfolding events out of 3840 curves in total SII-GFP-ybbR.
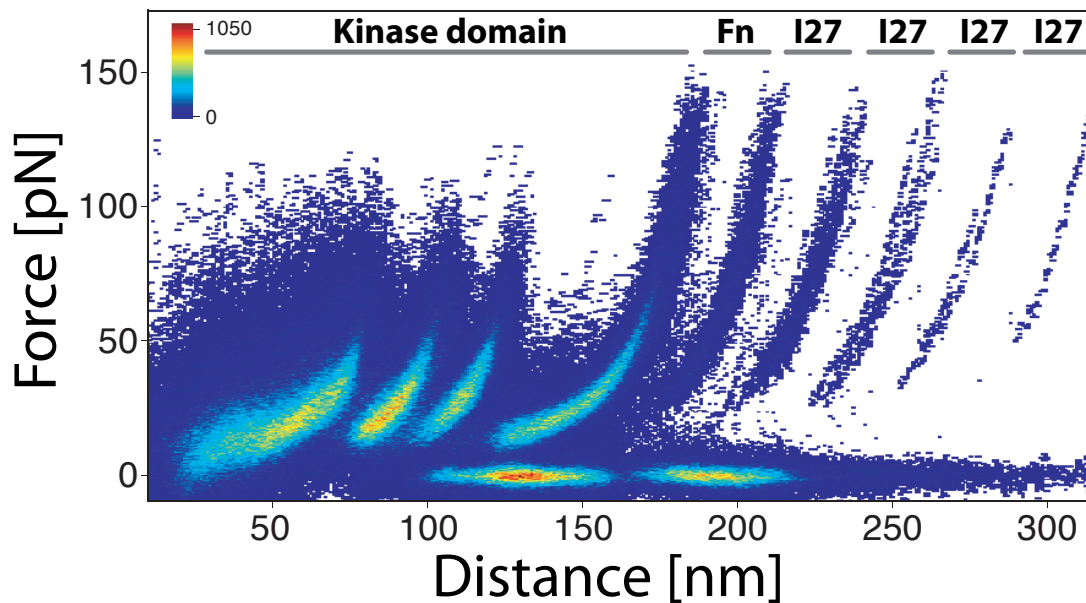
Supplementary Figure S5. Superposition of 1730 unfolding force vs. distance curves of a Titin Kinase construct (SII-I27-I27-Fn-Kinase-I27-I27-ybbR; I27 – Ig-like domain, Fn – Fibronectin domain) obtained by immobilization via a ybbR-tag and pulling via the SII-tag. Curves were obtained from measurements in five different retraction velocities (200, 800, 2000, 5000 and 10000 nm/s). The heat map illustrates data density. I27 unfolding is rarely observed as the required forces exceed the most probable rupture force of the SII:monoST interaction.

S11

Since TK proved to be a useful (low force) fingerprint to select and sort specific curves from the dataset, we could also perform a loading rate dependence analysis of the rupture force between N-terminally fused SII and monoST (Fig. 4B). The rupture forces for the C-terminally tagged GFP-SII fusion are about twice as high as for N-terminally SII-tagged TK. In agreement with this, the potential is broadened about twofold for the latter (Δx=0.45 nm vs. 0.23 nm for GFP-SII). K_{off} is in a comparable range for the two different geometries, taking into account that fusing SII to different proteins can already lead to large deviations (0.02-0.3 s^{-1} from surface plasmon resonance measurements for GFP-SII and Cytb$_{562}$-SII)[16]. It has to be noted, that no literature data exists concerning off-rates of an N-terminally SII-tagged protein from ST. For our ITC-based K_d measurements utilizing N- or C-terminally tagged GFP, values are in the same range at around 1 µM. The discrepancy in unbinding force for the different constructs can thus be more likely attributed to the altered pulling geometry.

Control measurements were carried out either employing a C-terminally GCN4-tagged GFP variant that was immobilized via the ybbR-tag on the surface (Supplementary Fig. S6), accordingly or by utilizing a ST construct on the cantilever that was completely devoid of a SII binding site. The fully mutated construct did not show any significant interaction, *i.e.* little interaction was observed and mainly single-WLC curves were obtained, likely originating from PEG stretching through unspecific interaction (data not shown). Further, desthiobiotin at 1mM concentration in the measurement buffer was used to block specific SII:monoST interactions (Supplementary Fig. S6). Even though initially GFP unfolding is still observed, the number of events is reduced compared to the data obtained before addition of the competitor, even more so over time when the competitor is fully diffused throughout the measurement buffer.

Successful coupling of ybbR-GFP constructs for control experiments and generally all measurements could be verified by detecting the GFP fluorescence on the surface (data not shown).
Further, the performance of monoST and tetraST in ybbR-GFP-SII force spectroscopy experiments was compared. Looking at the number of successful single-GFP unfolding events over time (illustrated by final rupture force vs. curve number) shows that the monoST construct is more stable over the entire measurement than the tetravalent version (Supplementary Fig. S7). A comparison of data yield for different measurements utilizing either tetra- or monoST is shown in Supplementary Table 1. A clear increase in yield of single event curves when employing the monovalent construct is evident. Remarkably,

S12

this is only looking at curves showing single GFP unfolding with subsequent SII/ST unbinding.
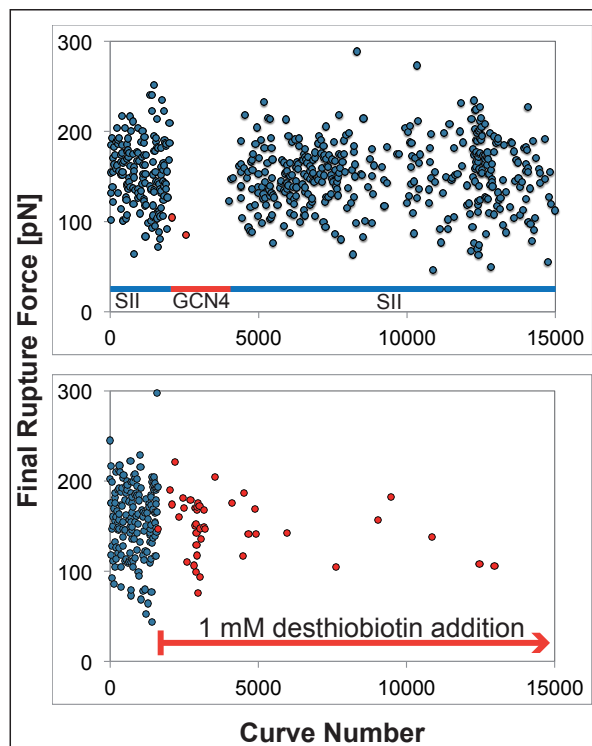
Supplementary Figure S6. Control and blocking experiments to validate specific SII:monoST interactions. The upper panel displays final SII:monoST unbinding forces (when a single GFP was unfolded) according to the curve number (at 10000 nm/s retraction velocity). First a GFP construct harbouring a C-terminal SII-tag was probed. After 2000 curves the same ST functionalized cantilever was moved to a position on the same glass surface where a GFP devoid of SII and harbouring a GCN4 peptide tag instead (also C-terminal) was immobilized. Again after another 2000 probing events the cantilever was moved back to the previous protein area. The lower panel depicts data obtained without and after addition of 1 mM desthiobition to the measurement buffer (same surface, same cantilever) that competes with the SII binding site.

Supplementary Table 1.Comparison of data yield from different AFM experiments. Exemplary measurements with tetraST and monoST were evaluated. For comparison data obtained with a retraction velocity of 5000 nm/s was taken into account. As the total number of collected curves varies, the ratio #single GFP unfolding events to #total curves is a good evaluation criterion.

measurement	#total curves	#single GFP unfolding events	Ratio [%]
Tetra I	8194	203	2.48
Tetra II	6531	170	2.60
Tetra III	8171	70	0.86
Tetra IV	10490	336	3.20
Mono I	8774	747	8.51
Mono II	6706	571	8.51
Mono III	10218	635	6.21

S13
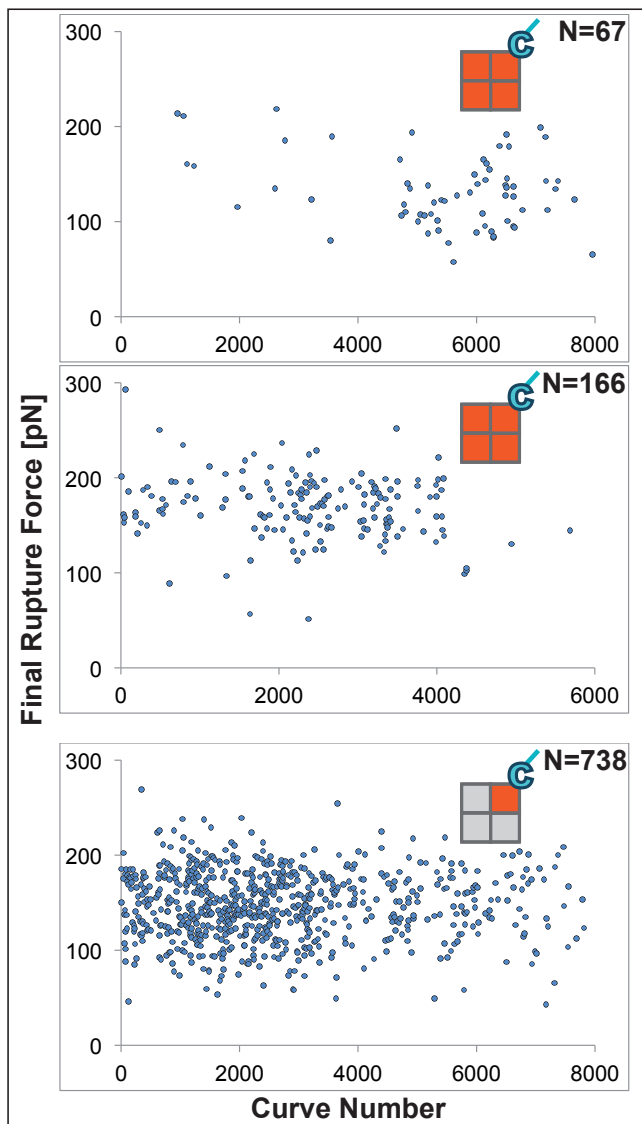
Supplementary Figure S7. Successful rupture event distribution during the course of a measurement. Final SII/ST unbinding forces are depicted (for single GFP unfolding events) according to the curve number throughout the experiment. Only curves from the sub data set with 5000 nm/s retraction velocity were evaluated. The upper two panels display exemplary data obtained with tetraST (8000 and 6000 curves total, respectively), the lower one with monoST (8000 curves total).

Construct sequences

6xHis-Cys-Strep-Tactin
MGSSHHHHHHMCGSEAGITGTWYNQLGSTFIVTAGADGALTGTYVTARGNAESRYVLTGRYDSAPATDGS
GTALGWTVAWKNNYRNAHSATTWSGQYVGGAEARINTQWLLTSGTTEANAWKSTLVGHDTFTKVKPSAAS

Non-functional Strep-Tactin
MEAGITGTWYAQLGRTFIVTAGADGALTGTYEAAMGNAESRYVLTGRYDSAPATDGSGTALGWTVAWKNNY
RNAHSATTWSGQYVGGAEARINTQWLLTSGTTEANAWKSTLVGHDTFTKVKPSAAS

ybbR-superfolderGFP-SII
GPLGSTMGSSHHHHHHSSGENLYFQGHMDSLEFIASKLAMSKGEELFTGVVPILVELDGDVNGHKFSVRGE
GEGDATIGKLTLKFICTTGKLPVPWPTLVTTLTYGVQCFSRYPDHMKRHDFFKSAMPEGYVQERTISFKDD
GKYKTRAVVKFEGDTLVNRIELKGTDFKEDGNILGHKLEYNFNSHNVYITADKQKNGIKANFTVRHNVEDG
SVQLADHYQQNTPIGDGPVLLPDNHYLSTQTVLSKDPNEKRDHMVLHEYVNAAGITHGMDELYKSGSGSAW
SHPQFEK

SII-TK-ybbR
MASWSHPQFEKGAETAVPNSPKSDVPIQAPHFKEELRNLNVRYQSNATLVCKVTGHPKPIVKWYRQ
GKEIIADGLKYRIQEFKGGYHQLIIASVTDDDATVYQVRATNQGGSVSGTASLEVEVPAKIHLPKT
LEGMGAVHALRGEVVSIKIPFSGKPDPVITWQKGQDLIDNNGHYQVIVTRSFTSLVFPNGVERKDA
GFYVVCAKNRFGIDQKTVELDVADVPDPPRGVKVSDVSRDSVNLTWTEPASDGGSKITNYIVEKCA
TTAERWLRVGQARETRYTVINLFGKTSYQFRVIAENKFGLSKPSEPSEPTITKEDKTRAMNYDEEV
DETREVSMTKASHSSTKELYEKYMIAEDLGRGEFGIVHRCVETSSKKTYMAKFVKVKGTDQVLVKK
EISILNIARHRNILHLHESFESMEELVMIFEFISGLDIFERINTSAFELNEREIVSYVHQVCEALQ
FLHSHNIGHFDIRPENIIYQTRRSSTIKIIEFGQARQLKPGDNFRLLFTAPEYYAPEVHQHDVVST
ATDMWSLGTLVYVLLSGINPFLAETNQQIIENIMNAEYTFDEEAFKEISIEAMDFVDRLLVKERKS
RMTASEALQHPWLKQKIERVSTKVIRTLKHRRYYHTLIKKDLNMVVSAARISCGGAIRSQKGVSVA
KVKVASIEIGPVSGQIMHAVGEEGGHVKYVCKIENYDQSTQVTWYFGVRQLENSEKYEITYEDGVA
ILYVKDITKLDDGTYRCKVVNDYGEDSSYAELFVKGVREVYDYYCRRTMKKIKRRTDTMRLLERPP
EFTLPLYNKTAYVGENVRFGVTITVHPEPHVTWYKSGQKIKPGDNDKKYTFESDKGLYQLTINSVT
TDDDAEYTVVARNKYGEDSCKAKLTVTLHPSSGSGGDSLEFIASKLASGLRGSHHHHHH

Abbreviations
AFM – atomic force microscopy; SMFS – single-molecule force spectroscopy; Cys –
Cysteine; SA/A – (Strept)avidin; ST – Strep-Tactin; monoST – monovalent Strep-Tactin;
tetraST – tetravalent Strep-Tactin; SII – Strep-tag II; ITC – isothermal titration
calorimetry; GFP – Green Fluorescent Protein; PEG – Polyethylenglycol

References

1.	Gumpp H, Stahl SW, Strackharn M, Puchner EM, Gaub HE. Ultrastable combined atomic force and total internal reflection fluorescence microscope [corrected]. *Rev Sci Instrum* 2009, **80**(6): 063704.

2.	Pedelacq JD, Cabantous S, Tran T, Terwilliger TC, Waldo GS. Engineering and characterization of a superfolder green fluorescent protein. *Nat Biotechnol* 2006, **24**(1): 79-88.

3.	Yin J, Lin AJ, Golan DE, Walsh CT. Site-specific protein labeling by Sfp phosphopantetheinyl transferase. *Nat Protoc* 2006, **1**(1): 280-285.

4.	Yin J, Straight PD, McLoughlin SM, Zhou Z, Lin AJ, Golan DE*, et al.* Genetically encoded short peptide tag for versatile protein labeling by Sfp phosphopantetheinyl transferase. *Proc Natl Acad Sci USA* 2005, **102**(44): 15815-15820.

5.	Pippig DA, Baumann F, Strackharn M, Aschenbrenner D, Gaub HE. Protein-DNA chimeras for nano assembly. *ACS nano* 2014, **8**(7): 6551-6555.

6.	Howarth M, Chinnapen DJ, Gerrow K, Dorrestein PC, Grandy MR, Kelleher NL*, et al.* A monovalent streptavidin with a single femtomolar biotin binding site. *Nat Methods* 2006, **3**(4): 267-273.

7.	Zimmermann JL, Nicolaus T, Neuert G, Blank K. Thiol-based, site-specific and covalent immobilization of biomolecules for single-molecule experiments. *Nature protocols* 2010, **5**(6): 975-985.

8.	Celik E, Moy VT. Nonspecific interactions in AFM force spectroscopy measurements. *Journal of molecular recognition : JMR* 2012, **25**(1): 53-56.

9.	Yin J, Lin AJ, Golan DE, Walsh CT. Site-specific protein labeling by Sfp phosphopantetheinyl transferase. *Nature protocols* 2006, **1**(1): 280-285.

10.	Moayed F, Mashaghi A, Tans SJ. A polypeptide-DNA hybrid with selective linking capability applied to single molecule nano-mechanical measurements using optical tweezers. *PloS one* 2013, **8**(1): e54440.

11.	Florin E. Sensing specific molecular interactions with the atomic force microscope. *Biosens Bioelectron* 1995, **10**(9-10): 895-901.

12.	Butt HJ, Jaschke M. Calculation of thermal noise in atomic-force microscopy. *Nanotechnology* 1995, **6**(1): 1-7.

13.	Hugel T, Rief M, Seitz M, Gaub HE, Netz RR. Highly stretched single polymers: atomic-force-microscope experiments versus ab-initio theory. *Phys Rev Lett* 2005, **94**(4): 048301.

14.	Evans E, Ritchie K. Dynamic strength of molecular adhesion bonds. *Biophys J* 1997, **72**(4): 1541-1555.

15.	Bell GI. Models for the specific adhesion of cells to cells. *Science* 1978, **200**(4342): 618-627.

16.	Schmidt TG, Batz L, Bonet L, Carl U, Holzapfel G, Kiem K*, et al.* Development of the Twin-Strep-tag(R) and its application for purification of recombinant proteins from cell culture supernatants. *Protein expression and purification* 2013, **92**(1): 54-61.